

Radial velocity variability fractions of different types of hot subdwarf stars

Ruijie He^{1,2}, Xiangcun Meng^{1,3,4}, Zhenxin Lei^{5,6}, Huahui Yan⁷, Shunyi Lan^{1,2}

¹ Yunnan Observatories, Chinese Academy of Sciences, Kunming 650011, PR China
e-mail: heruijie@ynao.ac.cn, xiangcunmeng@ynao.ac.cn

² University of the Chinese Academy of Sciences, Beijing 100049, PR China

³ Key Laboratory for the Structure and Evolution of Celestial Objects, Chinese Academy of Sciences, Kunming 650216, PR China

⁴ International Centre of Supernovae, Yunnan Key Laboratory, Kunming 650216, PR China

⁵ Key Laboratory of Stars and Interstellar Medium, Xiangtan University, Xiangtan 411105, PR China

⁶ Physics Department, Xiangtan University, Xiangtan 411105, PR China

⁷ Shandong Provincial Key Laboratory of Optical Astronomy and Solar-Terrestrial Environment, School of Space Science and Physics, Shandong University at Weihai, Weihai 264209, PR China

December 19, 2024

ABSTRACT

Context. It is generally thought that hot subdwarfs are helium-core- or helium-shell-burning objects with extremely thin hydrogen envelopes and that binary interactions are always needed in their formation. Different types of hot subdwarfs may have different origins, which will cause them to present different radial velocity (RV) variability properties.

Aims. We plan to study the RV-variability fractions of different types of hot subdwarfs, as well as their distributions in the $T_{\text{eff}} - \log g$ diagram. This provides insights into the formation of hot subdwarfs.

Methods. The cross-correlation function method was adopted to measure RV variations in 434 hot subdwarfs based on spectra obtained with the Large Sky Area Multi-Object Fiber Spectroscopic Telescope (LAMOST). Light curves from the Transiting Exoplanet Survey were also used to search for short-period binary hot subdwarfs.

Results. Only $6 \pm 4\%$ of our single-lined He-rich hot subdwarfs that only show spectroscopic features of hot subdwarfs are found to be RV variable, which is lower than the fraction of single-lined He-poor sdB stars ($31 \pm 3\%$). Single-lined sdB stars with effective temperatures (T_{eff}) $\sim 25,000 - 33,000$ K show an RV-variability fraction of $34 \pm 5\%$, while lower RV-variability fractions are observed for single-lined sdB stars cooler than about $25,000$ K ($11 \pm 4\%$), single-lined sdB/OB stars with $T_{\text{eff}} \sim 33,000 - 40,000$ K and surface gravities $\sim 5.7 - 6.0$ ($13 \pm 3\%$), as well as single-lined sdO/B stars with $T_{\text{eff}} \sim 45,000 - 70,000$ K ($10 \pm 7\%$). Single-lined hot subdwarfs with $T_{\text{eff}} \sim 35,000 - 45,000$ K located above the extreme horizontal branch (EHB) show a similar RV-variability fraction of $34 \pm 9\%$ as single-lined sdB stars at about $25,000 - 33,000$ K. The largest RV-variability fraction of $51 \pm 8\%$ is found in single-lined hot subdwarfs below the canonical EHB. The detected RV-variability fraction of our composite hot subdwarfs with an infrared excess in their spectral energy distributions is $9 \pm 3\%$, which is lower than that fraction of single-lined hot subdwarfs. Since the average RV uncertainty we measured in the LAMOST spectra is about 7.0 km/s, the lower detected RV-variability fraction for composite hot subdwarfs is expected because the RV amplitudes associated with long-period systems are lower.

Conclusions. The results here are generally consistent with the canonical binary evolution channels for forming hot subdwarfs. Most single-lined He-rich hot subdwarfs may form through merger channels, while the stable Roche-lobe overflow channel could play an important role in the formation of composite hot subdwarfs. Single-lined hot subdwarfs with $T_{\text{eff}} \sim 35,000 - 45,000$ K located above the EHB may have an evolutionary connection to the sdB stars at about $25,000 - 33,000$ K. The different detected RV-variability fractions for the different subclasses of single-lined hot subdwarfs indicate that their formation channels may differ.

Key words. stars:subdwarfs – stars:evolution – stars:binaries:general

1. Introduction

Most hot subdwarf stars are thought to be in the helium-core (He-core) or He-shell-burning stage. They are located at the extreme blue end of the horizontal branch (HB) in the Hertzsprung-Russell (HR) diagram and are also known as extreme horizontal branch (EHB) stars. The masses of canonical hot subdwarfs are about $0.5 M_{\odot}$ and their hydrogen envelopes are extremely thin ($< 0.02 M_{\odot}$) (Heber 1986). Their effective temperatures (T_{eff}) range between about $20,000 - 80,000$ K (see Heber 2009, 2016, for a detailed review). Hot subdwarfs play very important roles in many fields in astrophysics. They may be the main origin of the ultraviolet upturn in elliptical galaxies (Han et al. 2007). Short-period binaries that are composed of a hot subdwarf and a mas-

sive white dwarf (WD) are good candidates for the progenitors of type Ia supernovae (SNe Ia) (Maxted et al. 2000; Geier et al. 2007, 2013; Wang & Han 2010; Pelisoli et al. 2021). Additionally, some short-period binary hot subdwarfs with WD companions are also important gravitational wave (GW) sources for future studies (Kupfer et al. 2018; Lin et al. 2024).

About one-third of the hot subdwarfs are discovered in short-period, single-lined binaries (Maxted et al. 2001; Napiwotzki et al. 2004; Copperwheat et al. 2011; Kawka et al. 2015; Geier et al. 2022), which only present the spectroscopic features of hot subdwarfs. The orbital periods of these systems range from about one hour to several days, and their companions are mainly M-type main-sequence (dM), WD, or brown dwarf (BD) stars

(e.g., Kupfer et al. 2015; Schaffenroth et al. 2022). Another distinct type of stars from single-lined objects are composite hot subdwarfs. Because these objects usually have F-, G-, or K-type companions, an infrared (IR) excess can be detected in them (Heber et al. 2018; Solano et al. 2022). To date, all of the composite hot subdwarf binaries with orbital solutions were found to be long-period systems with periods from about 400 to 1,500 days (Vos et al. 2017, 2018, 2019).

In order to form hot subdwarfs, most of the hydrogen envelopes of their progenitors need to be lost before the He-core-burning phase. This mass loss is very difficult to achieve in the context of single-star evolution, and binary evolution is therefore usually proposed (Heber 2009, 2016). The detailed binary population synthesis (BPS) calculations from Han et al. (2002, 2003) indicated that stable Roche-lobe overflow (RLOF), common-envelope (CE) ejection, and double He-WD mergers are the main formation channels for hot subdwarfs. Long-period hot subdwarf binaries result from the stable RLOF channel (Han et al. 2002, 2003; Vos et al. 2020; Chen et al. 2013; Götberg et al. 2018). Short-period binary hot subdwarfs can only form through the CE ejection channel (Han et al. 2002, 2003; Xiong et al. 2017; Ge et al. 2024, 2022). The merger of double He-WDs in a short-period binary only produces single hot subdwarfs (Han et al. 2002, 2003; Webbink 1984; Zhang & Jeffery 2012; Hall & Jeffery 2016; Schwab 2018), and the merger products are typically considered to be He-rich hot subdwarfs (Zhang & Jeffery 2012; Schwab 2018). Additionally, some other models were proposed. When the merger occurs in a binary containing a red giant star (RGB) and a dM or BD companion, or even a high-mass planet during the CE phase, a rapidly rotating HB star may be produced (Kramer et al. 2020; Soker 1998; Politano et al. 2008). The centrifugal force for rapid rotation may enhance the mass loss from the HB star, and an sdB star may form. Justham et al. (2011) suggested that the merger of a hybrid CO-He WD and a He-WD can form He-sdO stars. Moreover, He-WDs that merge with their dM companions may initially form intermediate He-rich (iHe-rich) sdOB stars. Subsequently, the element diffusion processes may change them into He-poor sdOB stars (Zhang et al. 2017). Some single iHe-rich sdB stars might be surviving companions of SNe Ia from the WD+MS channel (e.g., Meng & Li 2019; Meng & Luo 2021).

Studies of radial velocity (RV) variable stars revealed that a substantial number of hot subdwarfs exist in short-period binaries. Furthermore, the RV-variability fractions differ among different types of hot subdwarfs, indicating that they may have different origins (e.g., Maxted et al. 2001; Napiwotzki et al. 2004; Copperwheat et al. 2011; Kawka et al. 2015; Geier et al. 2022). Maxted et al. (2001) observed 36 EHB stars over a time span of 11 nights to determine their RV variations. Among the five single-lined post-EHB stars and five composite EHB stars, only one single-lined post-EHB star was detected with significant RV variations. In contrast, a high RV-variability fraction of 68% was observed in their 26 single-lined EHB stars. Subsequently, by using the randomly observed spectra from the ESO Supernova Ia Progenitor Survey (SPY, Napiwotzki et al. 2001), Napiwotzki et al. (2004) found that the RV-variability fractions for 46 single-lined sdB and 23 single-lined He-sdO stars were 39% and 4%, respectively. The long-term monitoring survey conducted by Morales-Rueda et al. (2003) and Copperwheat et al. (2011) revealed that 64 out of 125 (51%) single-lined sdB stars and 5 out of 32 (16%) composite sdB stars exhibit RV variability. In summary, most He-rich hot subdwarfs usually do not show significant RV variations. Most composite hot subdwarfs are also not detected with significant RV variations based on the limited RV

accuracy achieved by low- or medium-resolution spectra. These two types of stars are quite different from the single-lined He-poor sdB stars.

Recently, Geier et al. (2022) have measured the RV variations for 646 single-lined hot subdwarfs by using the multi-epoch spectra from the Sloan Digital Sky Survey Data Release 12 (SDSS DR12, Alam et al. 2015) and the Large Sky Area Multi-Object Fiber Spectroscopic Telescope Data Release 5 (LAMOST DR5, Cui et al. 2012). Similar to some previous studies, almost all their He-rich hot subdwarfs were found to be non-RV variable. Moreover, they discovered that He-poor hot subdwarfs in different regions of the $T_{\text{eff}} - \log g$ diagram exhibit different RV-variability fractions. Cooler sdB stars ($< 24,000$ K) show a lower RV-variability fraction ($20^{+6}_{-4}\%$) than sdB stars with $T_{\text{eff}} \sim 25,000 - 32,000$ K ($34^{+3}_{-3}\%$). Hot subdwarfs with $T_{\text{eff}} \sim 32,000 - 40,000$ K ($34^{+3}_{-3}\%$) and surface gravities ($\log g \sim 5.6 - 6.0$) also show a lower RV-variability fraction ($22^{+4}_{-3}\%$), while the largest RV-variability fraction for hot subdwarfs below the EHB was discovered ($46^{+6}_{-6}\%$).

The RV variability of hot subdwarfs in observations is mainly influenced by their binary properties in short-period systems (e.g., Geier et al. 2022), which can help us to study the evolution of different types of hot subdwarfs and constrain their formation channels. To date, only Geier et al. (2022) have used a larger number of samples that contained different subclasses of hot subdwarfs to estimate the RV-variability fractions of hot subdwarfs along the different regions of the EHB. They discovered a different RV-variability fraction and origin for different subclasses of hot subdwarfs. However, the average uncertainty of the RV measurements in the study of Geier et al. (2022) is 18 km/s, which is somewhat large, and they only contained single-lined hot subdwarfs. To update the RV-variability fraction measurements of different subclasses of hot subdwarfs in Geier et al. (2022), and to discuss their possible formation channels, we simultaneously use the multi-epoch spectra from the LAMOST DR11 medium-resolution spectroscopic (MRS) surveys and the low-resolution spectroscopic (LRS) surveys here to measure the RV variations of hot subdwarfs. The structure of this paper is as follows. In Sect. 2 we introduce the sample selection and the RV measurement method. Sect. 3 briefly describes our results. A comparison and discussion are presented in Sect. 4, and our conclusions are given in Sect. 5.

2. Sample selection and radial velocity measurements

2.1. Sample selection

LAMOST is a 4m special reflecting Schmidt telescope with 4000 fibers. It is located at the Xinglong station of the National Astronomical Observatory (Cui et al. 2012; Zhao et al. 2012). Recently, LAMOST completed its regular survey observations for the first 11 years and published its 11th data release (DR11), which is not publicly available to all users. The LAMOST DR11 dataset contains 11,939,296 LRS and 13,187,912 MRS spectra. LAMOST LRS and MRS spectra have different spectral resolutions and wavelength ranges. LAMOST LRS spectra cover the wavelength range of 3690 – 9100 Å with a resolution of 1800 at 5500 Å, while LAMOST MRS spectra consist of two parts. The first part is the blue-arm spectrum, which covers 4950 – 5350 Å with a resolution of 7500 at 5163 Å, and the second part is the red-arm spectrum, which covers 6300 – 6800 Å with a resolution of 7500 at 6593 Å.

More than 6,500 hot subdwarfs have so far been confirmed by spectroscopy (Culpan et al. 2022; Geier 2020). Among them, many hot subdwarfs were identified through LAMOST LRS spectra (Lei et al. 2020, 2019, 2018; Luo et al. 2021, 2020, 2019, 2016), and these stars all have reliable atmospheric parameters, such as effective temperature, surface gravity, and surface helium abundance ($\log n(\text{He})/n(\text{H})$). In a recent study, Lei et al. (2023) newly identified 91 single-lined and 131 composite hot subdwarfs, which greatly increases the number of composite hot subdwarfs. All the hot subdwarfs identified in Lei et al. (2023, 2020, 2019, 2018) and Luo et al. (2021, 2020, 2019, 2016) were adopted as our initial samples. First, we cross-matched all the samples with the LAMOST DR11 MRS dataset. Hot subdwarfs with two or more observations in different nights were selected, and the criterion of the spectral signal-to-noise ratio (S/N) higher than 5 was employed to remove the poor-quality MRS spectra. Second, we cross-matched the remaining objects with the LAMOST DR11 LRS dataset. The spectral selection criteria for LRS are similar to those for MRS spectra, but with an $\text{S/N} > 10$ in the g band for LRS spectra.

2.2. Classifying the sample

2.2.1. Classification through the spectral energy distribution

Our sample consists of single-lined and composite hot subdwarfs. These two types of objects have distinct characteristics. Composite hot subdwarfs can show double-lined spectroscopic features, but they are sometimes very weak or cannot be detected. It is more efficient to detect IR excess in their spectral energy distributions (SEDs) to distinguish these objects. Recently, by using the Virtual Observatory SED Analyzer¹ (VOSA, Bayo et al. 2008) of the Spanish Virtual Observatory (SVO), Solano et al. (2022) built the largest SED database² of hot subdwarfs so far. It contains 3186 hot subdwarfs from the catalog of hot subdwarfs compiled by Geier (2020). Through the IR-excess characteristic of composite hot subdwarfs, Solano et al. (2022) classified 2469 stars as single-SED and 615 stars as composite-SED. To classify the single-lined and composite hot subdwarfs in our sample, we cross-matched our stars with the database of Solano et al. (2022), and obtained 109 composite and 365 single-lined hot subdwarfs. For a small portion of our hot subdwarfs that were not included in the database of Solano et al. (2022), we used VOSA to build their SEDs and classified them. The observed photometric data were collected from the following catalogs: the Galaxy Evolution Explorer (GALEX, Martin et al. 2005), the Panoramic Survey Telescope and Rapid Response System (Pan-STARRS DR2, Magnier et al. 2020), Gaia (Gaia Collaboration 2020), SDSS DR12 (Alam et al. 2015), the Two Micron All Sky Survey (2MASS, Skrutskie et al. 2006), and the Wide-field Infrared Survey Explorer (WISE, Wright et al. 2010).

2.2.2. Spectral classification

According to the traditional spectral classification scheme, hot subdwarfs can be divided into sdB, sdOB, sdO, He-sdB, He-sdOB, and He-sdO stars (Moehler et al. 1990; Geier et al. 2017). The classification criteria are as follows. SdB, sdOB, and sdO stars all have prominent hydrogen Balmer lines. SdB stars also show either no or weak He I lines, and sdOB stars usually show both weak He I and He II lines. SdO stars also have stronger

He II lines than the He I lines, but sometimes, no He I lines can be detected. On the other hand, all He-sdB and He-sdOB stars exhibit prominent He I lines. Additionally, He-sdOB stars have weak He II and hydrogen Balmer lines, while no He II lines can be detected in He-sdB stars. He-sdO stars show prominent He II lines together with weak or no He I and hydrogen Balmer lines.

Most of our hot subdwarfs were classified in the studies by Lei et al. (2023, 2020, 2019, 2018) and Luo et al. (2016) based on the spectral classification scheme described above. We adopted the classifications of these stars from the previous research. Additionally, a few hot subdwarfs from Luo et al. (2019, 2021) were not classified through the spectral line features. We inspected their spectra and classified them according to the traditional scheme.

2.3. Radial velocity measurements

Binary stars often show RV variations due to the Doppler effect that can be measured through spectral lines shifts. The cross-correlation function (CCF) method is often used to measure the RVs. This method calculates the RVs by cross-correlating template spectra with observed spectra (Yan et al. 2023; Li et al. 2021; Sana et al. 2013; Merle et al. 2017; Zhang et al. 2021). We used the algorithm of the CCF method as improved by Zhang et al. (2020, 2021) to calculate the RVs. Since the sharp $H\alpha$ lines and He I lines usually appear in the red arm of LAMOST MRS spectra and sometimes no obvious lines can be found in the blue-arm spectra, the red-arm MRS and LRS spectra were adopted as observed spectra.

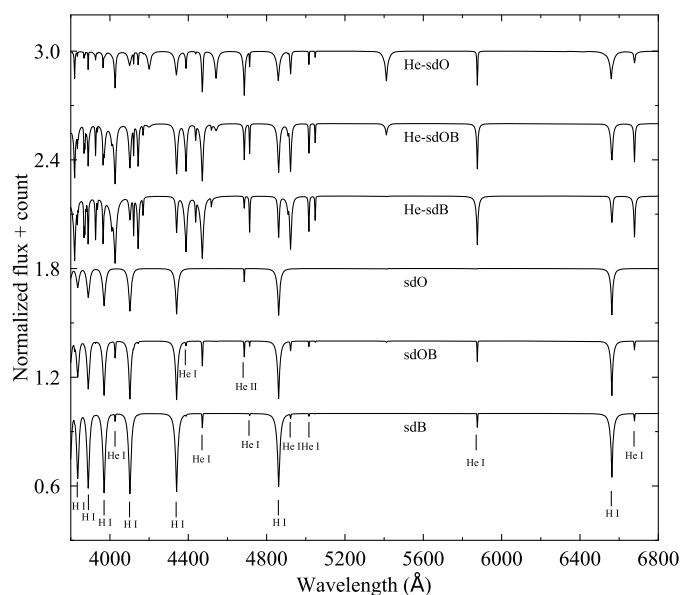


Fig. 1. Selected template spectra for six subtypes of hot subdwarfs from their synthetic spectra.

The synthetic spectra (SYNSPEC version 49, Lanz & Hubeny 2007) of hot subdwarfs calculated from nonlocal thermodynamic equilibrium (NLTE) TLUSTY model atmospheres (version 204, Hubeny & Lanz 2017) were adopted as our template. The template and observed spectra were normalized through the package LASPEC (Zhang et al. 2021). Based on the spectral classification, our hot subdwarfs were divided into six subtypes. In order to accurately measure their RVs, we selected one corresponding template for each type of hot subdwarf from their synthetic spectra. The classification of template spectra also

¹ <http://svo2.cab.inta-csic.es/svo/theory/vosa/>

² <http://svocats.cab.inta-csic.es/hsa2/>

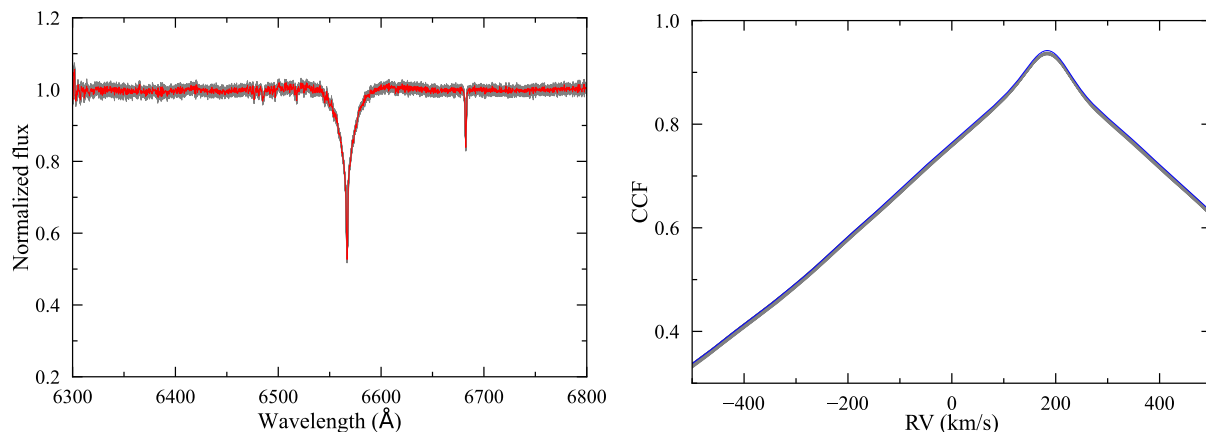


Fig. 2. Spectra normalization of the observed and simulated spectra together with their corresponding CCF curves. Left panel: Normalized observed spectrum (red line) and the 100 normalized simulated spectra (gray lines). Right panel: Original CCF curve (blue line) and the CCF curves of the 100 simulated spectra (gray lines).

followed the traditional scheme (Moehler et al. 1990; Geier et al. 2017). Our selected template spectra are shown in Fig. 1. Except for the hydrogen Balmer lines, the template spectra of sdB, sdOB, and sdO stars also have He I lines, both He I and He II lines, and He II lines, respectively. Except for the prominent He I lines for He-sdB and He-sdOB stars, and the prominent He II lines for He-sdO stars, the template spectra of He-sdOB and He-sdO stars also have He II and He I lines, respectively. Moreover, the template spectra of He-sdB, He-sdOB, and He-sdO stars all present detectable hydrogen Balmer lines. We cross-correlated the observed spectra of each type of hot subdwarf with their corresponding template, and the range of RV variations was set from -500 to 500 km/s with an interval of 1 km/s.

The spectral classification of our composite hot subdwarfs and the processes for measuring their RVs are the same as those that were used for single-lined objects. Some of our composite hot subdwarfs present double-lined features, but others only show an IR excess in their SEDs, and no spectral lines from the companions can be detected. In addition, the luminous hot subdwarfs contribute the majority of the flux for composite systems. Many double-lined composite hot subdwarfs show only weak lines of F-, G-, or K-type companions in the LAMOST LRS spectra. In this paper, we mainly focus on the primary component, and the RVs were only derived from the primary.

2.4. Radial velocity uncertainties

The Monte Carlo method was employed to estimate the uncertainties of our RV measurements (Yan et al. 2023; Li et al. 2021). For each flux at each wavelength point of the observed spectrum, 100 simulated flux values were randomly generated from a Gaussian distribution based on the flux and flux error. This allowed us to generate 100 simulated spectra for each observed spectrum. The 100 simulated spectra were used to calculate their CCF curves and RVs, and the standard deviation of the 100 RVs was taken as the RV uncertainty. The left panel of Fig. 2 shows the normalization of an observed red-arm MRS spectrum and 100 simulated spectra. Its right panel presents the original CCF curve and the 100 CCF curves derived through the simulated spectra. Since the systematic uncertainties are also induced by the stability of LRS/MRS over time spans of years, the spectral processing procedure, and so on, we added a systematic uncertainty of 5 km/s in quadrature to all the RV uncertainties mea-

sured from the LRS/MRS spectra to calculate their final uncertainties (Geier et al. 2024, 2022).

To obtain as many reliable RVs as possible and to explore the RV-variability fractions of different subclasses of hot subdwarfs with relatively smaller RV uncertainties, we set a limit to select stars with RV uncertainties smaller than 15 km/s. Furthermore, the CCF maximum of each observed spectrum was restricted to be larger than 0.15 (Merle et al. 2017). Eventually, we obtained the multi-epoch RVs for 434 hot subdwarfs, of which 45 are from the MRS spectra and 389 are from the LRS spectra. Fig. 3 presents the distributions of σ_v for these stars. The average σ_v obtained from the LRS and MRS spectra is 7.6 km/s and 5.6 km/s, respectively, and the average σ_v obtained from all the LRS and MRS spectra is 7.1 km/s.

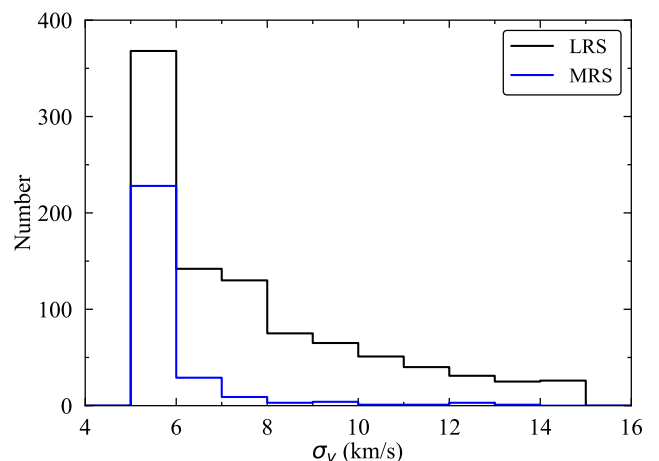


Fig. 3. Radial velocity uncertainty distributions of hot subdwarfs. The black line shows the RV uncertainties measured from the LRS spectra, and the blue line represents the RV uncertainties measured from the MRS spectra.

3. Distribution of radial velocity variations and variability criterion

3.1. Distribution of radial velocity variations

Our final sample consisted of 317 single-lined and 117 composite hot subdwarfs. The maximum RV variation (ΔRV_{\max}) was

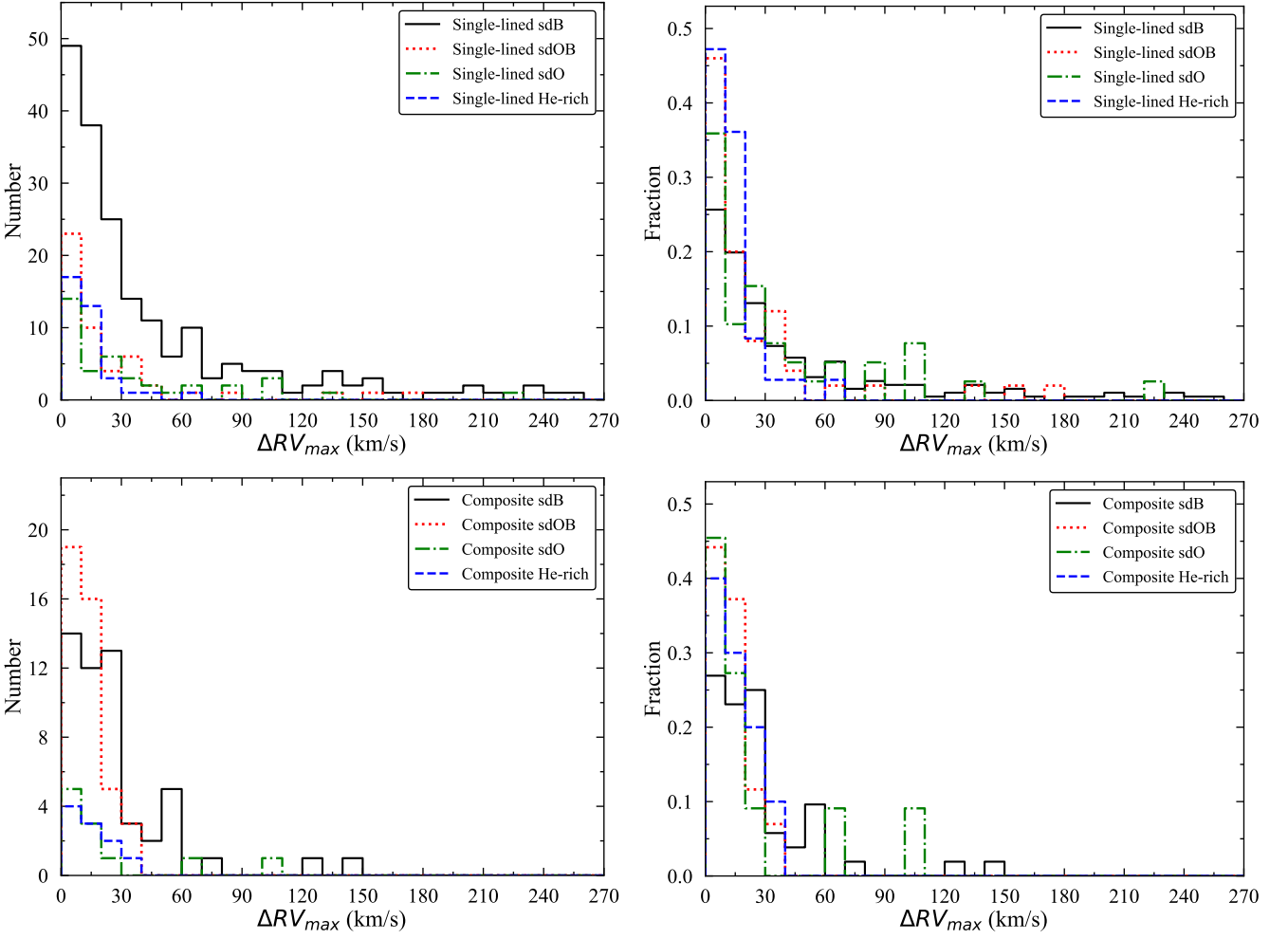


Fig. 4. ΔRV_{\max} distributions of different types of hot subdwarfs. Left panels: Absolute numbers in each bin. Right panels: Normalized fractions in the same bin as in the left panels. The solid black, dotted red, dash-dotted green, and dashed blue lines in the upper panels represent the ΔRV_{\max} distributions for single-lined sdB, sdOB, sdO, and He-rich hot subdwarfs. The same types of lines in the bottom panels show the ΔRV_{\max} distributions of composite sdB, sdOB, sdO, and He-rich hot subdwarfs, respectively.

Table 1. RV-variability fractions of different types of hot subdwarfs and a comparison with Geier et al. (2022).

Subtype	Total	RV-variable	Fraction (%)	Total (Geier)	RV-variable (Geier)	Fraction (Geier) (%)
all single-lined	317	79	25 ± 2	646	164	25 ± 2
sdB	191	60	31 ± 3	378	120	32 ± 2
sdOB	51	7	14 ± 5	117	29	25 ± 4
sdO	39	10	26 ± 7	44	12	27 ± 7
He-rich	36	2	6 ± 4	107	3	3 ± 2
all composite	117	10	9 ± 3	–	–	–
sdB	52	8	15 ± 5	–	–	–
sdOB	44	0	0_{-0}^{+1}	–	–	–
sdO	11	2	18 ± 12	–	–	–
He-rich	10	0	0_{-0}^{+5}	–	–	–

calculated by subtracting the minimum from the maximum RV of the star. In the upper panels of Fig. 4, we show the ΔRV_{\max} distributions of single-lined sdB, sdOB, sdO, and He-rich hot subdwarfs. All single-lined He-rich hot subdwarfs have helium abundances of $\log n(\text{He})/n(\text{H}) > -1$. We found that single-lined He-rich hot subdwarfs obviously exhibit more fractions of stars with ΔRV_{\max} lower than 20 km/s compared to single-lined sdB stars. In order to assess the statistical difference of this comparison, the

Kolmogorov-Smirnov (K-S) test was employed. We obtained a P_{KS} value of 9×10^{-6} , which indicates that the ΔRV_{\max} distributions of single-lined sdB and He-rich hot subdwarfs are not from the same mother sample. Moreover, more than 600 He-rich hot subdwarfs were discovered, but only a few special He-rich hot subdwarfs were found in short-period binaries (Ahmad et al. 2004; Şener & Jeffery 2014; Lisker et al. 2004; Ratzloff et al. 2020; Reindl et al. 2020; Kupfer et al. 2017b, 2020a,b; Snow-

don et al. 2023). Most of them are very special stars, which may originate from the CE ejection of intermediate-mass stars when they cross the Hertzsprung gap (Kupfer et al. 2020a,b) or come from the CE ejection of post-early asymptotic giant branch stars (AGB, Li et al. 2024). The majority of He-rich hot subdwarfs are very unlikely to form through these rare and peculiar channels. Our results support the opinions of Geier et al. (2022) and other researchers that most He-rich hot subdwarfs may be single stars, and merger channels such as the double He-WDs merger may lead to their formation, which can explain their surface helium enrichment and ΔRV_{\max} distributions well.

In the bottom panels of Fig. 4, we show the ΔRV_{\max} distributions of composite sdB, sdOB, sdO, and He-rich hot subdwarfs. We found that composite sdB and sdOB stars exhibit a smaller fraction of stars with ΔRV_{\max} higher than 60 km/s than their corresponding type of single-lined hot subdwarfs. The KS-test showed a statistically significant difference in the ΔRV_{\max} distributions between composite sdB and single-lined sdB stars ($P_{\text{KS}} = 4.9 \times 10^{-4}$), which indicates that these two types of stars belong to different populations. Nevertheless, except that no composite sdOB stars show ΔRV_{\max} higher than 60 km/s, the ΔRV_{\max} distributions in 0 – 40 km/s for composite sdOB and single-lined sdOB stars are similar. The KS-test does not reveal a statistically significant difference in the ΔRV_{\max} distributions between these two types of stars either ($P_{\text{KS}} = 0.20$). Based on the limited RV accuracy achieved by LAMOST LRS/MRS spectra, it is hard to detect an obvious difference between the ΔRV_{\max} distributions of composite and single-lined sdOB stars. More observations with higher-accuracy RVs may be needed to reveal whether their ΔRV_{\max} distributions differ. Because the sample size of composite sdO and composite He-rich hot subdwarfs is limited, the statistical analysis for these stars may not be reliable. We just present their ΔRV_{\max} distributions as a reference.

3.2. Criterion for radial velocity variability

We adopted the same method as used by Maxted et al. (2001), Geier et al. (2022, 2024), Napiwotzki et al. (2020), and Yan et al. (2024) to estimate the probability of a star that is variable in RV. First, we calculated the weighted mean RV of every star and assumed the value as a constant. Then, we calculated the χ^2 statistic. By comparing the calculated χ^2 with the χ^2 distribution for the appropriate degrees of freedom, we calculated the probability (p) of obtaining the observed χ^2 value or a higher value from random fluctuations of a constant velocity. Stars that showed a false detection p lower than 0.01% ($\log p < -4$) were considered to be significantly RV-variable objects. In Table A.1 we present the RV variability and other parameters of our sample.

3.3. Variability fractions in different types of hot subdwarfs

In the upper part of Table 1, we list the RV-variability fractions of different types of single-lined hot subdwarfs based on our study and Geier et al. (2022). The data catalog³ of Geier et al. (2022) also contains the spectral classifications of 646 hot subdwarfs based on the scheme of Moehler et al. (1990), which were adopted by us for the sample of Geier et al. (2022), and hot subdwarfs with $\log n(\text{He})/n(\text{H}) > -1$ were classified as He-rich. The uncertainties in the RV-variability fractions were derived based on the assumption of a binomial distribution, while the uncertainties for the subtypes without detected RV-variable

stars were estimated by using the beta distribution to calculate the 68% confidence upper limit. It should be noted that the RV-variability fractions of different types of hot subdwarfs are just their lower limits since some sources only have a small number of RV measurements, and the long-period hot subdwarf binaries are difficult to detect with significant RV variations.

The detected RV-variability fractions of our single-lined sdB, sdO, and He-rich hot subdwarfs are all consistent with the fractions from the sample of Geier et al. (2022) within the uncertainties. Only two of our single-lined He-rich hot subdwarfs are found to be RV variable. They are PG 1415+492 and BD+48 1777, and they exhibit RV variations of 64 km/s and 33 km/s, respectively. These two special stars may be in short-period binaries and currently lack available orbital solutions. They deserve further observations to study their formation. The RV-variability fraction of our single-lined sdOB stars is $14 \pm 5\%$, which is lower than the fraction of single-lined sdB stars. A somewhat higher RV-variability fraction of $25 \pm 4\%$ is found in the single-lined sdOB stars of Geier et al. (2022). It is slightly lower than that fraction of their single-lined sdB stars within the uncertainties. A detailed discussion of the RV variability of single-lined sdOB stars is presented in Sect. 4.1.

The bottom part of Table 1 presents the RV-variability fractions of different types of composite hot subdwarfs. We found that $9 \pm 3\%$ of all our composite hot subdwarfs exhibit significant RV variations, which is lower than the fraction of $25 \pm 2\%$ for all single-lined hot subdwarfs. The RV-variability fractions of our composite sdB and sdOB are also lower than their corresponding type of single-lined stars. Currently, 27 composite hot subdwarfs possess solved orbital parameters (Vos et al. 2012, 2013, 2017, 2019; Deca et al. 2012; Barlow et al. 2012, 2013; Østensen & Van Winckel 2012; Molina et al. 2022; Németh et al. 2021; Dorsch et al. 2021). All of them are long-period binaries with periods longer than 400 days. Since the average uncertainty of our RV measurements from LAMOST spectra is about 7 km/s, the lower detected RV-variability fraction for composite hot subdwarfs is expected because most of them may be long-period binaries, which is consistent with the supposition of Copperwheat et al. (2011).

Our results support that most composite hot subdwarfs are in long-period binaries, and the stable RLOF channel may be their main formation channel (e.g., Pelisoli et al. 2020; Vos et al. 2020). However, there still exist some special cases, in which 8 of our composite sdB stars and 2 of our composite sdO stars exhibit significant RV variations. These stars all show RV variations larger than 45 km/s, and LAMOSTJ 073756.25+311646.5, PG 1629+081, and GALEXJ 071314.5+173459 all show RV variations larger than 100 km/s. Similar to our study, 5 composite sdB stars were also detected with significant RV variations in the 32 composite sdB stars (16%) of Copperwheat et al. (2011). The RV variations of these composite hot subdwarfs might be caused by the following several reasons. First, the evolutionary pathways from triple systems were proposed to produce hot subdwarfs, and a great number of hot subdwarfs from these scenarios were predicted to be in triple systems (Preece et al. 2022). In observations, several triple-system candidates were also discovered (Heber et al. 2002; Kupfer et al. 2015; Pelisoli et al. 2020; Schaffenroth et al. 2023). These stars are composed of an inner short-period hot subdwarf binary with an unseen companion and a distant F-, G-, or K-type companion. The RV-variable composite hot subdwarfs could be in such triple systems, and they might be triple-system candidates. Second, some of these stars might be blends, and they are not real composite hot subdwarf binaries. Third, although all the composite hot subdwarfs with solved or-

³ <http://cdsarc.u-strasbg.fr/viz-bin/cat/J/A+A/661/A113>

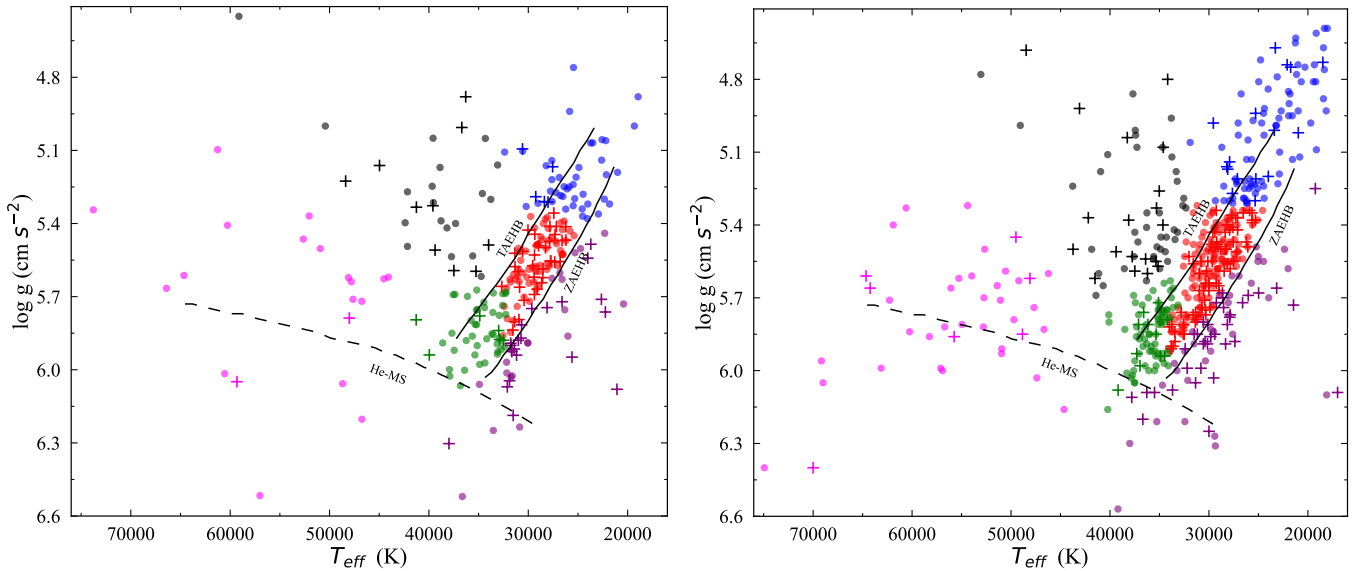


Fig. 5. $T_{\text{eff}} - \log g$ diagram of different subclasses of single-lined He-poor hot subdwarfs. The left panel shows our sample, and the right panel shows the sample of Geier et al. (2022). The circles represent non-RV-variable hot subdwarfs, and the crosses represent RV-variable hot subdwarfs. The sample is divided into six subclasses that are marked by different colors, for which EHBa, EHBb, EHBc, bEHBa, postEHBa, and postEHBb are plotted in blue, red, green, purple, black, and magenta, respectively. The zero-age EHB (ZAEHB) and terminal-age EHB (TAEHB) sequences with $Z = 0.02$ from Dorman et al. (1993) are labeled by solid black lines. The helium main sequence (He-MS) from Paczyński (1971) is marked by the dashed black line.

Table 2. RV-variability fractions for the six subclasses of hot subdwarfs and a comparison with Geier et al. (2022).

Subclass	Total	RV-variable	Fraction (%)	Total(Geier)	RV-variable (Geier)	Fraction (Geier) (%)
EHBa	47	5	11 ± 4	92	16	17 ± 4
EHBb	96	33	34 ± 5	195	72	37 ± 3
EHBc	48	6	13 ± 5	84	11	13 ± 4
bEHBa	41	21	51 ± 8	69	36	52 ± 6
postEHBa	29	10	34 ± 9	60	19	32 ± 6
postEHBb	20	2	10 ± 7	39	7	18 ± 6

bital parameters were proven to be long-period binaries, we still cannot exclude the possibility that these RV-variable composite hot subdwarfs are in short-period binaries with F-, G-, or K-type companions (Copperwheat et al. 2011). Because we only have a few RV measurements of these composite hot subdwarfs, the nature of the companions cannot be defined. More follow-up observations are needed to reveal the properties of these stars.

4. Comparison and discussion

4.1. Distribution in the $T_{\text{eff}} - \log g$ diagram

Geier et al. (2022) discovered that the RV-variability fractions of single-lined He-poor hot subdwarfs in different regions of the $T_{\text{eff}} - \log g$ diagram are different. In Fig. 5 we compared the distributions of our single-lined He-poor hot subdwarfs with those of Geier et al. (2022). All the atmospheric parameters of our hot subdwarfs are from the previously identified works (Lei et al. 2023, 2020, 2019, 2018; Luo et al. 2021, 2020, 2019, 2016). Similar to the division criteria of Geier et al. (2022) but with some differences, we divided hot subdwarfs into six subclasses (EHBa, EHBb, EHBc, bEHBa, postEHBa, and postEHBb) through visual inspection of their locations in the $T_{\text{eff}} - \log g$ diagram and the density of the RV-variable together with non-RV-variable stars, as well as their spectral types. A detailed discussion is given in the following subsections. The statistics

for the RV-variability fractions of these subclasses from our sample and that of Geier et al. (2022) are shown in Table 2. Our RV-variability fractions for the six subclasses are consistent with those of Geier et al. (2022) within the uncertainties, although we implemented a stricter restriction that limited the RV uncertainties to less than 15 km/s.

4.1.1. Stars along the extreme horizontal branch

As shown in Fig. 5, EHBa, EHBb, and EHBc stars are all distributed along the EHB. Almost all the EHBa and EHBb are sdB stars. There seems to be a change in the density of RV-variable stars at $T_{\text{eff}} \sim 25,000$ K and $\log g \sim 5.3$, which divides the majority of sdB stars into EHBa and EHBb. The RV-variability fraction of EHBa stars based on our sample and on that of Geier et al. (2022) is $11 \pm 4\%$ and $17 \pm 4\%$. Both values are lower than the fraction of $34 \pm 5\%$ and $37 \pm 3\%$ for EHBb stars. Geier et al. (2022) first noted that the cooler sdB stars present a lower RV-variability fraction than the higher-temperature group. This distribution trend for RV-variable sdB stars is consistent with the prediction of BPS simulations from Han et al. (2003) that the CE ejection channel can only form a few sdB stars cooler than about 25,000 K. Based on the lower RV-variability fraction and the BPS simulations, Geier et al. (2022) speculated that the cooler group of sdB stars may contain a new subpopulation

of long-period binaries with late-type MS or compact companions. Moreover, the simulations of the stable RLOF channel from Vos et al. (2020) indicated that about one-third of the sdB stars from this channel are long-period single-lined binaries with late-type MS companions, and sdB stars with $T_{\text{eff}} \sim 20,000$ K can be produced. This further supports the supposition of Geier et al. (2022). In addition, some of the cooler sdB stars may also have been created through merger channels, such as the merger of an RGB star with its companion (Politano et al. 2008).

The classification for EHBb and EHBc stars is based on their spectral types. A boundary exists between sdB and sdOB stars at $T_{\text{eff}} \sim 33,000$ K. Hot subdwarfs in the region of the sdOB stars grouping are classified as EHBc, and they also contain a few sdB stars. We separated the EHBc and postEHBa stars through the small density gap of sdOB stars at $\log g \sim 5.7$. The RV-variability fraction of EHBc stars (with $T_{\text{eff}} \sim 33,000 - 40,000$ K and $\log g \sim 5.7 - 6.0$) from our sample and that of Geier et al. (2022) shows a lower value of $13 \pm 5\%$ and $13 \pm 4\%$ compared to EHBb stars. Geier et al. (2022) also found that hot subdwarfs of their EHB3 group, which are located in a similar region to our EHBc stars, exhibited a lower RV-variability fraction than their EHB2 group. They suggested two possible reasons for the lower RV-variability fraction. The first reason was that their EHB3 sample might be populated by some single iHe-sdOB stars with inaccurate helium abundance measurements. However, as shown in Fig. 3 of Luo et al. (2021), they obtained quite consistent helium abundance measurements with Lei et al. (2018, 2019, 2020) ranging from $-2 < \log n(\text{He})/n(\text{H}) < 0$. In Fig. 6 we present the distributions of our single-lined hot subdwarfs in the two different helium abundance ranges. The figure clearly shows that most EHBc stars have helium abundances in the range of $-2 < \log n(\text{He})/n(\text{H}) \leq -1$. We therefore think that the majority of helium abundance measurements for our EHBc stars are accurate enough. The alternative explanation provided by Geier et al. (2022) is that the non-RV-variable stars in their EHB3 group might evolve from single iHe-rich hot subdwarfs by diffusion processes as proposed by Miller Bertolami et al. (2008). Most of our EHBc stars exhibit higher helium abundances of $\log n(\text{He})/n(\text{H})$ than EHBb stars. This is consistent with the prediction of Miller Bertolami et al. (2008) based on diffusion processes. The higher helium abundances as well as the lower RV-variability fraction of EHBc stars all support an evolutionary connection between iHe-rich hot subdwarfs and EHBc stars.

4.1.2. Stars above and beyond the extreme horizontal branch

The division between postEHBa and EHBa, b, and c stars is mainly based on their density and locations. Hot subdwarfs located above the EHB and separate from EHBa, b, and c stars are classified as postEHBa. There seems to be a density gap of stars at $T_{\text{eff}} \sim 45,000$ K that divides hot subdwarfs above and beyond the EHB into two subclasses. The lower-temperature group with $T_{\text{eff}} \sim 35,000 - 45,000$ K is labeled as postEHBa, and the higher-temperature group with $T_{\text{eff}} \sim 45,000 - 70,000$ K is labeled as postEHBb. We found that the RV-variability fraction of postEHBa stars from our sample and that of Geier et al. (2022) is $34 \pm 9\%$ and $34 \pm 6\%$. Both values are close to the fraction of EHBb stars. Since only a few postEHBa stars are predicted to form through the CE ejection channel based on the BPS simulations from Han et al. (2003), these stars may have an evolutionary connection to EHBb stars. Nevertheless, postEHBb stars show a lower RV-variability fraction of $10 \pm 7\%$ and $18 \pm 6\%$ based on our sample and on that of Geier et al. (2022). The evolutionary process that begins from EHBb stars and then connects to

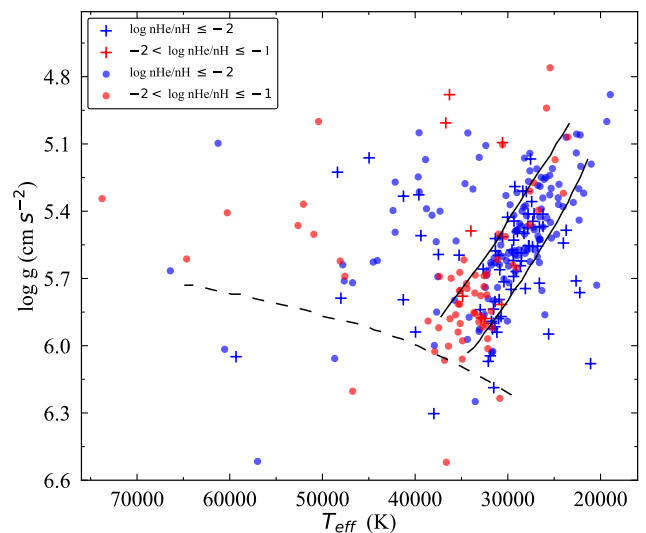


Fig. 6. Distributions of single-lined He-poor hot subdwarfs with different helium abundances. The hot subdwarfs with helium abundances of $\log n(\text{He})/n(\text{H})$ in the two different ranges are labeled by different colors. Same as Fig. 5, the circles represent non-RV-variable hot subdwarfs, and the crosses represent RV-variable hot subdwarfs.

postEHBb stars might not apply to all postEHBb stars. One possible scenario for their formation is that some non-RV-variable postEHBb stars might evolve from the single He-sdO stars by diffusion processes (Miller Bertolami et al. 2008).

4.1.3. Stars below the extreme horizontal branch

Hot subdwarfs below the canonical ZAEHB are classified as bEHBa. Because the location of ZAEHB derived through the evolutionary tracks has some uncertainties that depend on the metallicity and helium-core mass of the stars (Dorman et al. 1993; Geier et al. 2022), we did not strictly constrain our bEHBa stars to be below the ZAEHB. Some stars on the line or very close to it were also classified as bEHBa. The bEHBa stars based on our sample and Geier et al. (2022) show the largest RV-variability fraction of $51 \pm 8\%$ and $52 \pm 6\%$. Geier et al. (2022) also noted the high RV-variability fraction of hot subdwarfs below the EHB. They suggested that the concentration of hotter stars ($> 25,000$ K) below the EHB might be composed of low-mass hot subdwarfs that evolved from the intermediate-mass stars with ignited nondegenerate helium cores, while several more widely distributed cooler stars might be progenitors of He-WDs with non-core helium burning (a detailed discussion can be seen in Geier et al. (2022)). Based on the high RV-variability fraction and the locations of our bEHBa stars, we support that the majority of these stars might be low-mass hot subdwarfs, especially the concentration of bEHBa stars at $T_{\text{eff}} \sim 30,000$ K, while the cooler bEHBa stars ($< 25,000$ K) and the bEHBa stars below the He-MS might be progenitors of He-WDs.

4.2. Comparison with short-period binary hot subdwarfs from light curves and the literature

4.2.1. Collecting short-period binaries

Many hot subdwarfs show different types of variability in their light curves due to binarity or pulsations. Short-period binary hot subdwarfs with low-mass MS or BD companions can exhibit quasi-sinusoidal variability in their light curves owing to

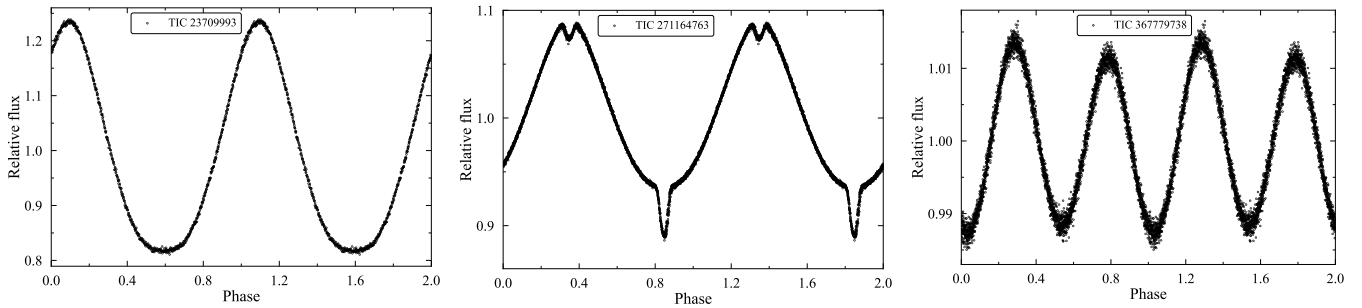


Fig. 7. Light curves of different types of light-variable hot subdwarfs. The light curves of a reflection effect and a HW Vir system in the first and second panels are phase-folded to the orbital period. The third panel shows the light curve of an ellipsoidal deformation system phase-folded to twice the orbital period.

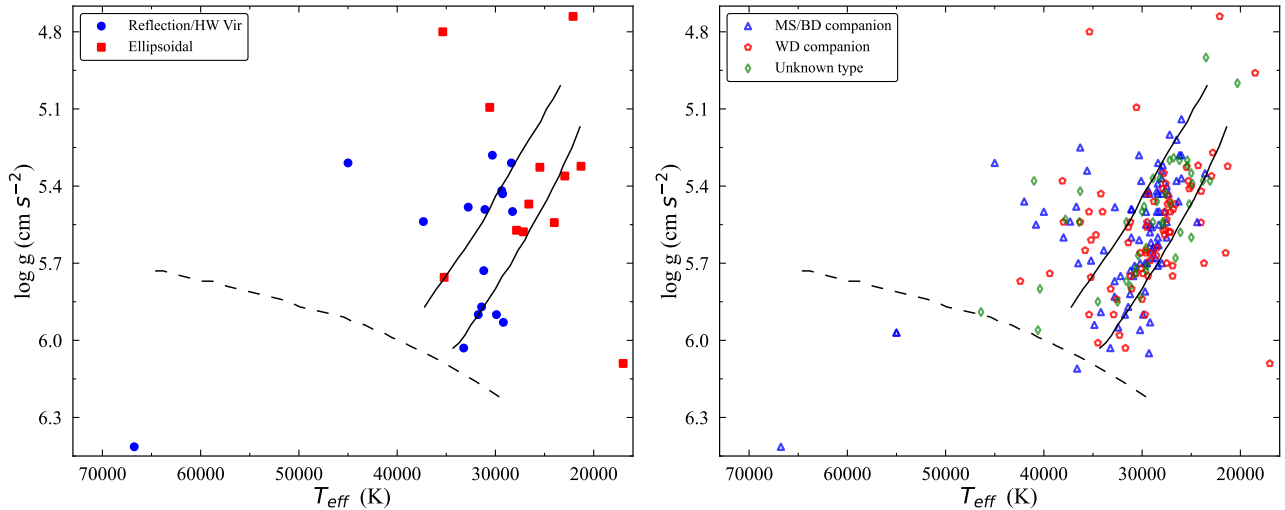


Fig. 8. $T_{\text{eff}} - \log g$ diagram of the confirmed short-period binary hot subdwarfs from light curves and the literature. Left panel: Newly found reflection effect or HW Vir systems (blue circles) and the newly discovered ellipsoidal deformation systems (red squares). Right panel: Known short-period binary hot subdwarfs in the literature and our newly found short-period binaries through light curves. Hot subdwarfs with MS or BD companions and WD companions are labeled as blue triangles and red pentagons, respectively. Short-period binary hot subdwarfs with an unknown companion type are labeled as green diamonds.

the reflection effect, and HW Vir systems are eclipsing reflection effect systems (Schaffenroth et al. 2022, 2023; Wang et al. 2023; Baran et al. 2021; Barlow et al. 2022). Compact hot subdwarf binaries with WD companions can show ellipsoidal deformation (Pelisoli et al. 2021; Lin et al. 2024; Kupfer et al. 2022). Additionally, many hot subdwarfs show variability due to pulsations, with typical periods of a few minutes or about one to two hours (Kupfer et al. 2021; Baran et al. 2023, 2024).

Space-based telescope observations like the Transiting Exoplanet Survey Satellite (TESS, Ricker et al. 2015) and the K2 space missions (Howell et al. 2014) are very efficient in obtaining a large number of high-quality light curves for many stars. Schaffenroth et al. (2022) used light curves from TESS and K2 to search for short-period binary hot subdwarfs. They detected 82 new sdB+dM/BD and 23 new sdB+WD systems. It is quite interesting to investigate whether there is any difference for the distributions in the $T_{\text{eff}} - \log g$ diagram between RV-variable hot subdwarfs and other confirmed short-period binary hot subdwarfs. To achieve this comparison, we used the 2-minute cadence and 20-second cadence light curves from TESS to search for short-period binary hot subdwarfs in the single-lined samples of Lei et al. (2018, 2019, 2020, 2023); Luo et al. (2016, 2019, 2020, 2021), and Geier et al. (2022). Following the data reduction method used by Schaffenroth et al. (2022),

we adopted the publicly available custom script⁴ developed by Pelisoli et al. (2020) to download light curves and generate periodograms. Subsequently, we phase-folded the light curves to the period determined by the periodogram or twice the period for ellipsoidal deformation systems. Example light curves of a reflection effect, a HW Vir, and an ellipsoidal deformation system are presented in Fig. 7. After conducting visual inspections for the light curves of 593 hot subdwarfs, we newly discovered 12 reflection effect, 4 HW Vir, and 12 ellipsoidal deformation systems that were previously unknown. These stars are plotted in the left panel of Fig. 8. In Table A.2 we present the period and other parameters of these stars.

The right panel of Fig. 8 shows the distributions of known short-period binary hot subdwarfs with atmospheric parameters in the literature (Schaffenroth et al. 2022, 2019, 2018, 2015, 2013; Baran et al. 2019; Kupfer et al. 2017a, 2020b; Ratzloff et al. 2019; Østensen et al. 2010; Kawka et al. 2015; Geier et al. 2014, 2011, 2010; Copperwheat et al. 2011; Maxted et al. 2001; Kupfer et al. 2015, and references therein), as well as our newly discovered short-period binaries through light curves. The companions of short-period binary hot subdwarfs are mainly dM, BD, or WD stars. We also present the distributions of these two

⁴ <https://github.com/ipelisoli/TESS-LS>

types of hot subdwarfs by blue triangles and red pentagons. We found that they exhibit a quite similar distribution in the $T_{\text{eff}} - \log g$ diagram.

4.2.2. Comparison

In Fig. 9 we combine the RV-variable hot subdwarfs (213) from our study and Geier et al. (2022) and compare their distributions with the confirmed short-period binary hot subdwarfs (210) from light curves and the literature. The two distributions are quite similar, except that more RV-variable stars are located below the He-MS. Only $5 \pm 1\%$, $6 \pm 2\%$, and $1 \pm 1\%$ of the confirmed short-period binaries are found in the region in which EHBa, EHBc, and postEHBb stars are located, which is consistent with

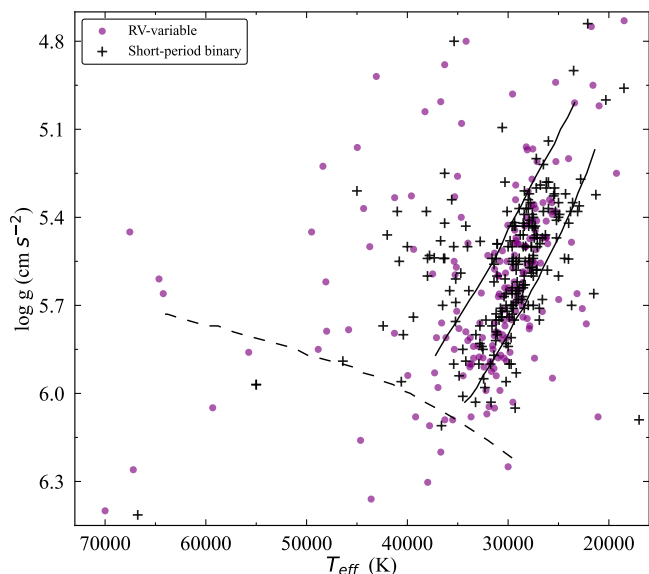


Fig. 9. Distributions of RV-variable hot subdwarfs and the confirmed short-period binary hot subdwarfs from light curves and the literature in the $T_{\text{eff}} - \log g$ diagram. The black crosses represent the confirmed short-period hot subdwarfs. The purple circles represent RV-variable hot subdwarfs.

the lower possibility of RV-variable stars to appear in these regions ($7 \pm 2\%$, $7 \pm 2\%$, $6 \pm 2\%$). We found that $11 \pm 2\%$ of the confirmed short-period binaries are grouped in the region in which post-EHBa stars are located. The value is similar to the fraction of $12 \pm 2\%$ for RV-variable stars that appear in the region. As we mentioned before, these stars may have an evolutionary connection to EHBb stars. In addition, the simulations of Dorman et al. (1993) predicted that the EHB stars should spend most of their lifetimes during the He-shell burning stage at $T_{\text{eff}} \sim 35,000 - 50,000$ K, and then quickly evolve to the WD cooling stage. This means that these He-shell-burning stars which evolved from the EHB stars are more likely to be observed to cluster at the lower-temperature region above the EHB.

5. Summary and conclusions

We have measured the RV variations of 317 single-lined and 117 composite hot subdwarfs through LAMOST DR11 LRS and MRS spectra. These stars were classified into different types according to their spectral line features and helium abundances to explore their RV-variability fractions. By combining our sample with that of Geier et al. (2022), we studied the relation between the RV-variability of hot subdwarfs and their locations

in the $T_{\text{eff}} - \log g$ diagram. The light-variable hot subdwarfs searched through TESS light curves and the known short-period binary hot subdwarfs were also used to verify our results. The basic results are similar to those in Geier et al. (2022), and we summarize them as follows.

1. Only $6 \pm 4\%$ of single-lined He-rich hot subdwarfs are found to be RV-variable. Their RV-variability fraction is significantly lower than that of single-lined He-poor sdB stars. Most of them may form through merger channels.
2. Single-lined sdB stars with $T_{\text{eff}} \sim 25,000 - 33,000$ K show an RV-variability fraction of $34 \pm 5\%$, whereas single-lined sdB stars cooler than about 25,000 K ($11 \pm 4\%$) and single-lined sdB/OB stars with $T_{\text{eff}} \sim 33,000 - 40,000$ K and $\log g \sim 5.7 - 6.0$ ($13 \pm 3\%$) all exhibit a lower RV-variability fraction.
3. The detected RV-variability fraction for single-lined hot subdwarfs that are located above the EHB band with $T_{\text{eff}} \sim 35,000 - 45,000$ K is $34 \pm 9\%$. The value is similar to the fraction of sdB stars at about 25,000 – 33,000 K. These two subclasses of hot subdwarfs may have an evolutionary connection. However, single-lined hot subdwarfs stars with $T_{\text{eff}} \sim 45,000 - 70,000$ K show a lower RV-variability fraction of $10 \pm 7\%$. Some of them may not be connected to the evolution of sdB stars.
4. Single-lined hot subdwarfs located below the canonical EHB show the largest RV-variability fraction of $51 \pm 8\%$. The majority of these stars may be low-mass hot subdwarfs or progenitors of He-WDs.
5. The detected RV-variability fraction of composite hot subdwarfs ($9 \pm 3\%$) is lower than the single-lined hot subdwarfs ($25 \pm 2\%$). The stable RLOF channel may play an important role in the formation of composite hot subdwarfs.
6. Eight composite sdB and two composite sdO stars were detected with RV variations larger than 45 km/s. These stars might be triple-system candidates or blends, and they require further observations to reveal their properties.

Data availability

Table A.1 is only available in electronic form at the CDS via anonymous ftp to cdsarc.u-strasbg.fr (130.79.128.5) or via <http://cdsweb.u-strasbg.fr/cgi-bin/qcat?J/A+A/>.

Acknowledgements. We thank the useful advice from Stephan Geier and Veronika Schaffenroth. This work is supported by the National Natural Science Foundation of China (Nos. 12288102 and 12333008) and National Key R&D Program of China (No. 2021YFA1600403). X.M. acknowledges support from Yunnan Fundamental Research Projects (Nos. 202401BC070007 and 202201BC070003), International Centre of Supernovae, Yunnan Key Laboratory (No. 202302AN360001), the Yunnan Revitalization Talent Support Program Science & Technology Champion Project (NO. 202305AB350003), and the science research grants from the China Manned Space Project. Thanks to the LAMOST excellent spectra. The LAMOST Fellowship is supported by Special Funding for Advanced Users, budgeted and administered by the Center for Astronomical Mega-Science, Chinese Academy of Sciences (CAMs). Guoshoujing Telescope (the Large Sky Area Multi Object Fiber Spectroscopic Telescope LAMOST) is a National Major Scientific Project built by the Chinese Academy of Sciences. Funding for the project has been provided by the National Development and Reform Commission.

References

- Ahmad, A., Jeffery, C. S., & Fullerton, A. W. 2004, *A&A*, 418, 275
 Alam, S., Albareti, F. D., Allende Prieto, C., et al. 2015, *ApJS*, 219, 12
 Arancibia-Rojas, E., Zorotovic, M., Vučković, M., et al. 2024, *MNRAS*, 527, 11184
 Baran, A. S., Charpinet, S., Østensen, R. H., et al. 2024, *A&A*, 686, A65

- Baran, A. S., Sahoo, S. K., Sanjayan, S., & Ostrowski, J. 2021, *MNRAS*, 503, 3828
- Baran, A. S., Telting, J. H., Jeffery, C. S., et al. 2019, *MNRAS*, 489, 1556
- Baran, A. S., Van Grootel, V., Østensen, R. H., et al. 2023, *A&A*, 669, A48
- Barlow, B. N., Corcoran, K. A., Parker, I. M., et al. 2022, *ApJ*, 928, 20
- Barlow, B. N., Liss, S. E., Wade, R. A., & Green, E. M. 2013, *ApJ*, 771, 23
- Barlow, B. N., Wade, R. A., Liss, S. E., Østensen, R. H., & Van Winckel, H. 2012, *ApJ*, 758, 58
- Bayo, A., Rodrigo, C., Barrado Y Navascués, D., et al. 2008, *A&A*, 492, 277
- Bloemen, S., Hu, H., Aerts, C., et al. 2014, *A&A*, 569, A123
- Chen, X., Han, Z., Deca, J., & Podsiadlowski, P. 2013, *MNRAS*, 434, 186
- Copperwheat, C. M., Morales-Rueda, L., Marsh, T. R., Maxted, P. F. L., & Heber, U. 2011, *MNRAS*, 415, 1381
- Şener, H. T. & Jeffery, C. S. 2014, *MNRAS*, 440, 2676
- Cui, X.-Q., Zhao, Y.-H., Chu, Y.-Q., et al. 2012, *Research in Astronomy and Astrophysics*, 12, 1197
- Culpan, R., Geier, S., Reindl, N., et al. 2022, *A&A*, 662, A40
- Deca, J., Marsh, T. R., Østensen, R. H., et al. 2012, *MNRAS*, 421, 2798
- Derekas, A., Németh, P., Southworth, J., et al. 2015, *ApJ*, 808, 179
- Dorman, B., Rood, R. T., & O'Connell, R. W. 1993, *ApJ*, 419, 596
- Dorsch, M., Jeffery, C. S., Irrgang, A., Woolf, V., & Heber, U. 2021, *A&A*, 653, A120
- Gaia Collaboration. 2020, *VizieR Online Data Catalog: Gaia EDR3 (Gaia Collaboration, 2020)*, *VizieR On-line Data Catalog: I/350*. Originally published in: 2021A&A...649A...1G. doi:10.5270/esa-lug
- Ge, H., Tout, C. A., Chen, X., et al. 2022, *ApJ*, 933, 137
- Ge, H., Tout, C. A., Webbink, R. F., et al. 2024, *ApJ*, 961, 202
- Geier, S. 2020, *A&A*, 635, A193
- Geier, S., Dorsch, M., Pelisoli, I., et al. 2022, *A&A*, 661, A113
- Geier, S., Heber, U., Irrgang, A., et al. 2024, *A&A*, 690, A368
- Geier, S., Heber, U., Podsiadlowski, P., et al. 2010, *A&A*, 519, A25
- Geier, S., Hirsch, H., Tillich, A., et al. 2011, *A&A*, 530, A28
- Geier, S., Marsh, T. R., Wang, B., et al. 2013, *A&A*, 554, A54
- Geier, S., Nesslinger, S., Heber, U., et al. 2007, *A&A*, 464, 299
- Geier, S., Østensen, R. H., Heber, U., et al. 2014, *A&A*, 562, A95
- Geier, S., Østensen, R. H., Németh, P., et al. 2017, *A&A*, 600, A50
- Götberg, Y., de Mink, S. E., Groh, J. H., et al. 2018, *A&A*, 615, A78
- Hall, P. D. & Jeffery, C. S. 2016, *MNRAS*, 463, 2756
- Han, Z., Podsiadlowski, P., & Lynas-Gray, A. E. 2007, *MNRAS*, 380, 1098
- Han, Z., Podsiadlowski, P., Maxted, P. F. L., & Marsh, T. R. 2003, *MNRAS*, 341, 669
- Han, Z., Podsiadlowski, P., Maxted, P. F. L., Marsh, T. R., & Ivanova, N. 2002, *MNRAS*, 336, 449
- Heber, U. 1986, *A&A*, 155, 33
- Heber, U. 2009, *ARA&A*, 47, 211
- Heber, U. 2016, *PASP*, 128, 082001
- Heber, U., Irrgang, A., & Schaffenroth, J. 2018, *Open Astronomy*, 27, 35
- Heber, U., Moehler, S., Napiwotzki, R., Thejll, P., & Green, E. M. 2002, *A&A*, 383, 938
- Howell, S. B., Sobek, C., Haas, M., et al. 2014, *PASP*, 126, 398
- Hubeny, I. & Lanz, T. 2017, *arXiv e-prints*, arXiv:1706.01859
- Justham, S., Podsiadlowski, P., & Han, Z. 2011, *MNRAS*, 410, 984
- Kawka, A., Vennes, S., O'Toole, S., et al. 2015, *MNRAS*, 450, 3514
- Kramer, M., Schneider, F. R. N., Ohlmann, S. T., et al. 2020, *A&A*, 642, A97
- Kupfer, T., Bauer, E. B., Burdge, K. B., et al. 2020a, *ApJ*, 898, L25
- Kupfer, T., Bauer, E. B., Marsh, T. R., et al. 2020b, *ApJ*, 891, 45
- Kupfer, T., Bauer, E. B., van Roestel, J., et al. 2022, *ApJ*, 925, L12
- Kupfer, T., Geier, S., Heber, U., et al. 2015, *A&A*, 576, A44
- Kupfer, T., Korol, V., Shah, S., et al. 2018, *MNRAS*, 480, 302
- Kupfer, T., Prince, T. A., van Roestel, J., et al. 2021, *MNRAS*, 505, 1254
- Kupfer, T., Ramsay, G., van Roestel, J., et al. 2017a, *ApJ*, 851, 28
- Kupfer, T., van Roestel, J., Brooks, J., et al. 2017b, *ApJ*, 835, 131
- Lanz, T. & Hubeny, I. 2007, *ApJS*, 169, 83
- Lei, Z., He, R., Németh, P., et al. 2023, *ApJ*, 942, 109
- Lei, Z., Zhao, J., Németh, P., & Zhao, G. 2018, *ApJ*, 868, 70
- Lei, Z., Zhao, J., Németh, P., & Zhao, G. 2019, *ApJ*, 881, 135
- Lei, Z., Zhao, J., Németh, P., & Zhao, G. 2020, *ApJ*, 889, 117
- Li, C.-q., Shi, J.-r., Yan, H.-l., et al. 2021, *ApJS*, 256, 31
- Li, Z., Zhang, Y., Chen, H., et al. 2024, *ApJ*, 964, 22
- Lin, J., Wu, C., Xiong, H., et al. 2024, *Nature Astronomy*, 8, 491
- Lisker, T., Heber, U., Napiwotzki, R., et al. 2004, *Ap&SS*, 291, 351
- Luo, Y., Németh, P., Deng, L., & Han, Z. 2019, *ApJ*, 881, 7
- Luo, Y., Németh, P., & Li, Q. 2020, *ApJ*, 898, 64
- Luo, Y., Németh, P., Wang, K., Wang, X., & Han, Z. 2021, *ApJS*, 256, 28
- Luo, Y.-P., Németh, P., Liu, C., Deng, L.-C., & Han, Z.-W. 2016, *ApJ*, 818, 202
- Magnier, E. A., Schlafly, E. F., Finkbeiner, D. P., et al. 2020, *ApJS*, 251, 6
- Martin, D. C., Fanson, J., Schiminovich, D., et al. 2005, *ApJ*, 619, L1
- Maxted, P. F. L., Heber, U., Marsh, T. R., & North, R. C. 2001, *MNRAS*, 326, 1391
- Maxted, P. F. L., Marsh, T. R., & North, R. C. 2000, *MNRAS*, 317, L41
- Meng, X. & Li, J. 2019, *MNRAS*, 482, 5651
- Meng, X.-C. & Luo, Y.-P. 2021, *MNRAS*, 507, 4603
- Merle, T., Van Eck, S., Jorissen, A., et al. 2017, *A&A*, 608, A95
- Miller Bertolami, M. M., Althaus, L. G., Unglaub, K., & Weiss, A. 2008, *A&A*, 491, 253
- Miller Bertolami, M. M., Battich, T., Córscico, A. H., Althaus, L. G., & Wachlin, F. C. 2022, *MNRAS*, 511, L60
- Moehler, S., Richtler, T., de Boer, K. S., Dettmar, R. J., & Heber, U. 1990, *A&AS*, 86, 53
- Molina, F., Vos, J., Németh, P., et al. 2022, *A&A*, 658, A122
- Morales-Rueda, L., Maxted, P. F. L., Marsh, T. R., North, R. C., & Heber, U. 2003, *MNRAS*, 338, 752
- Napiwotzki, R., Christlieb, N., Drechsel, H., et al. 2001, *Astronomische Nachrichten*, 322, 411
- Napiwotzki, R., Karl, C. A., Lisker, T., et al. 2020, *A&A*, 638, A131
- Napiwotzki, R., Karl, C. A., Lisker, T., et al. 2004, *Ap&SS*, 291, 321
- Németh, P. 2020, *Contributions of the Astronomical Observatory Skalnaté Pleso*, 50, 546
- Németh, P., Vos, J., Molina, F., & Bastian, A. 2021, *A&A*, 653, A3
- Østensen, R. H., Green, E. M., Bloemen, S., et al. 2010, *MNRAS*, 408, L51
- Østensen, R. H. & Van Winckel, H. 2012, in *Astronomical Society of the Pacific Conference Series*, Vol. 452, *Fifth Meeting on Hot Subdwarf Stars and Related Objects*, ed. D. Kilkenny, C. S. Jeffery, & C. Koen, 163
- Paczynski, B. 1971, *Acta Astron.*, 21, 1
- Pelisolì, I., Neunteufel, P., Geier, S., et al. 2021, *Nature Astronomy*, 5, 1052
- Pelisolì, I., Vos, J., Geier, S., Schaffenroth, V., & Baran, A. S. 2020, *A&A*, 642, A180
- Politano, M., Taam, R. E., van der Sluys, M., & Willems, B. 2008, *ApJ*, 687, L99
- Preece, H. P., Hamers, A. S., Battich, T., & Rajamuthukumar, A. S. 2022, *MNRAS*, 517, 2111
- Ratzloff, J. K., Barlow, B. N., Kupfer, T., et al. 2019, *ApJ*, 883, 51
- Ratzloff, J. K., Kupfer, T., Barlow, B. N., et al. 2020, *ApJ*, 902, 92
- Reindl, N., Schaffenroth, V., Miller Bertolami, M. M., et al. 2020, *A&A*, 638, A93
- Ricker, G. R., Winn, J. N., Vanderspek, R., et al. 2015, *Journal of Astronomical Telescopes, Instruments, and Systems*, 1, 014003
- Sana, H., de Koter, A., de Mink, S. E., et al. 2013, *A&A*, 550, A107
- Schaffenroth, V., Barlow, B. N., Drechsel, H., & Dunlap, B. H. 2015, *A&A*, 576, A123
- Schaffenroth, V., Barlow, B. N., Geier, S., et al. 2019, *A&A*, 630, A80
- Schaffenroth, V., Barlow, B. N., Pelisoli, I., Geier, S., & Kupfer, T. 2023, *A&A*, 673, A90
- Schaffenroth, V., Geier, S., Drechsel, H., et al. 2013, *A&A*, 553, A18
- Schaffenroth, V., Geier, S., Heber, U., et al. 2018, *A&A*, 614, A77
- Schaffenroth, V., Pelisoli, I., Barlow, B. N., Geier, S., & Kupfer, T. 2022, *A&A*, 666, A182
- Schwab, J. 2018, *MNRAS*, 476, 5303
- Skrutskie, M. F., Cutri, R. M., Stiening, R., et al. 2006, *AJ*, 131, 1163
- Snowdon, E. J., Jeffery, C. S., Schlagenhauf, S., Dorsch, M., & Monageng, I. M. 2023, *MNRAS*, 525, 183
- Soker, N. 1998, *AJ*, 116, 1308
- Solano, E., Ulla, A., Pérez-Fernández, E., et al. 2022, *MNRAS*, 514, 4239
- Vennes, S., Kawka, A., O'Toole, S. J., Németh, P., & Burton, D. 2012, *ApJ*, 759, L25
- Vos, J., Bobrick, A., & Vučković, M. 2020, *A&A*, 641, A163
- Vos, J., Németh, P., Vučković, M., Østensen, R., & Parsons, S. 2018, *MNRAS*, 473, 693
- Vos, J., Østensen, R. H., Degroote, P., et al. 2012, *A&A*, 548, A6
- Vos, J., Østensen, R. H., Németh, P., et al. 2013, *A&A*, 559, A54
- Vos, J., Østensen, R. H., Vučković, M., & Van Winckel, H. 2017, *A&A*, 605, A109
- Vos, J., Vučković, M., Chen, X., et al. 2019, *MNRAS*, 482, 4592
- Wang, B. & Han, Z.-W. 2010, *Research in Astronomy and Astrophysics*, 10, 681
- Wang, K., Kupfer, T., & Barlow, B. N. 2023, *MNRAS*, 524, 3769
- Webbink, R. F. 1984, *ApJ*, 277, 355
- Wright, E. L., Eisenhardt, P. R. M., Mainzer, A. K., et al. 2010, *AJ*, 140, 1868
- Wu, Y., Chen, X., Li, Z., & Han, Z. 2018, *A&A*, 618, A14
- Xiong, H., Chen, X., Podsiadlowski, P., Li, Y., & Han, Z. 2017, *A&A*, 599, A54
- Yan, H., Zhao, J., Shi, W., et al. 2024, *A&A*, 684, A103
- Yan, H.-H., Zhao, J.-K., Shi, W.-B., et al. 2023, *Universe*, 9, 177
- Zhang, B., Li, J., Yang, F., et al. 2021, *ApJS*, 256, 14
- Zhang, B., Liu, C., & Deng, L.-C. 2020, *ApJS*, 246, 9
- Zhang, X., Hall, P. D., Jeffery, C. S., & Bi, S. 2017, *ApJ*, 835, 242
- Zhang, X. & Jeffery, C. S. 2012, *MNRAS*, 419, 452
- Zhao, G., Zhao, Y.-H., Chu, Y.-Q., Jing, Y.-P., & Deng, L.-C. 2012, *Research in Astronomy and Astrophysics*, 12, 723

Appendix A: Additional material**Table A.1.** The RV variations and atmospheric parameters of 434 hot subdwarfs.

R.A. (deg)	Decl. (deg)	T_{eff} (K)	$\log g$ (cm s^{-2})	$\log n(\text{He})/n(\text{H})$	Single-lined	Spclass	$\log p$	Epoch (Number)	ΔRV_{max} (km/s)
194.455489	54.42649	33130 ± 150	5.89 ± 0.02	-1.55 ± 0.04	is	sdOB	-0.001	9	3 ± 7
257.555047	53.446121	24010 ± 440	5.54 ± 0.11	-2.13 ± 0.11	is	sdB	-14.78	2	89 ± 11
56.022214	22.072953	28130 ± 440	5.59 ± 0.06	-2.74 ± 0.09	is	sdB	-3.02	7	40 ± 9
71.237089	14.363909	32660 ± 320	5.66 ± 0.05	-2.49 ± 0.13	is	sdB	-7.84	2	64 ± 11
98.497308	32.553966	26010 ± 1210	5.86 ± 0.11	-2.97 ± 0.42	is	sdB	-2.88	3	43 ± 16
...
62.954352	15.383123	37490 ± 520	5.59 ± 0.04	-3.23 ± 0.15	is	sdO	-15.95	4	106 ± 16

(This table is available in its entirety at the CDS. The uncertainty of ΔRV_{max} is propagated from the uncertainties of its corresponding maximum and minimum RV.)

Table A.2. The main parameters of our newly discovered short-period binary hot subdwarfs through light curves.

R.A. (deg)	Decl. (deg)	T_{eff} (K)	$\log g$ (cm s^{-2})	$\log n(\text{He})/n(\text{H})$	Spclass	TIC (ID)	Type	Period (h)
346.401764	34.698363	28260 ± 160	5.50 ± 0.02	-2.34 ± 0.04	sdB	369581468	Reflection	4.77
345.4409	13.64374	31190 ± 220	5.73 ± 0.05	-1.74 ± 0.04	sdB	217587019	Reflection	3.92
312.413176	30.081818	37330 ± 170	5.54 ± 0.06	-2.58 ± 0.12	sdOB	230775376	Reflection	10.31
4.23055	51.230486	32770 ± 460	5.48 ± 0.07	-3.04 ± 0.58	sdB	202125132	Reflection	6.50
93.23016	57.847462	29270 ± 270	5.43 ± 0.03	-2.28 ± 0.04	sdB	322550178	Reflection	3.09
118.30847	11.211171	29360 ± 60	5.42 ± 0.01	-2.44 ± 0.04	sdB	468928859	Reflection	6.39
352.34432	32.233162	31070 ± 280	5.49 ± 0.07	-2.59 ± 0.26	sdB	2054270826	Reflection	4.23
29.0050281	40.0561321	28380 ± 330	5.31 ± 0.03	-2.62 ± 0.04	sdB	67423472	Reflection	4.65
207.719937	36.700612	66760 ± 2380	6.41 ± 0.07	-1.07 ± 0.22	sdO	23709993	Reflection	79.55
77.542438	30.11271	29192 ± 263	5.93 ± 0.06	-2.29 ± 0.09	sdB	367014246	Reflection	2.75
103.90969	31.394393	33232 ± 466	6.03 ± 0.11	-1.96 ± 0.14	sdOB	741122759	Reflection	3.42
321.634188	-4.223943	31412 ± 220	5.87 ± 0.05	-2.82 ± 0.09	sdB	250262974	Reflection	4.48
109.74026	7.653687	45003 ± 731	5.31 ± 0.05	-2.74 ± 0.13	sdO	264749962	HW Vir	2.03
114.89894	56.709241	29896 ± 553	5.90 ± 0.11	-2.49 ± 0.12	sdB	742806233	HW Vir	8.20
316.00591	34.610072	30312 ± 644	5.28 ± 0.14	-2.70 ± 0.07	sdB	1957912171	HW Vir	2.85
356.26688	50.965145	31748 ± 329	5.90 ± 0.09	-2.63 ± 0.16	sdB	26994998	HW Vir	1.94
257.555047	53.446121	24010 ± 440	5.54 ± 0.11	-2.13 ± 0.11	sdB	367779738	Ellipsoidal	1.82
288.815187	43.674379	27850 ± 240	5.57 ± 0.04	-2.55 ± 0.04	sdB	158918567	Ellipsoidal	2.44
94.486139	18.83019	26600 ± 480	5.47 ± 0.05	-2.91 ± 0.15	sdB	429807453	Ellipsoidal	2.06
181.601508	57.159922	35220 ± 350	5.76 ± 0.04	-1.75 ± 0.06	sdOB	55753808	Ellipsoidal	9.98
8.943925	26.915094	27150 ± 520	5.58 ± 0.06	-2.44 ± 0.09	sdB	301799840	Ellipsoidal	10.46
332.511298	25.066193	21290 ± 80	5.32 ± 0.02	-2.39 ± 0.04	sdB	27782233	Ellipsoidal	4.00
317.098329	1.032085	25480 ± 500	5.33 ± 0.04	-2.50 ± 0.06	sdB	387373406	Ellipsoidal	14.10
117.04874	13.730365	22940 ± 930	5.36 ± 0.16	-2.68 ± 0.34	sdB	17561485	Ellipsoidal	3.76
91.999515	13.6144053	30580 ± 1510	5.09 ± 0.02	-1.57 ± 0.12	sdB	151473446	Ellipsoidal	15.68
159.265844	-0.138644	35357 ± 415	4.80 ± 0.04	-2.51 ± 0.13	sdB	124598476	Ellipsoidal	44.56
238.9077349	27.1134627	22100 ± 900	4.74 ± 0.10	-3.00 ± 0.10	sdB	258109545	Ellipsoidal	155.26
292.2527216	44.9497531	17001 ± 94	6.09 ± 0.02	-2.43 ± 0.13	sdB	63208546	Ellipsoidal	7.10